The Aeronautical Journal (2024), **128**, pp. 2105–2125
doi:10.1017/aer.2024.32

ROYAL AERONAUTICAL SOCIETY

RESEARCH ARTICLE

Altering flight stability characteristics of a high-performance aircraft through wing strake modification

H. Raza[1], A. Maqsood[2] and J. Masud[3]

[1]School of Interdisciplinary Engineering and Science (SINES), NUST, Islamabad, Pakistan
[2]National University of Sciences and Technology, Islamabad, Pakistan
[3]Air University, Islamabad, Pakistan
Corresponding author: A. Maqsood; Email: adnan@sines.nust.edu.pk

Received: 14 August 2023; **Revised:** 28 January 2024; **Accepted:** 13 March 2024

Keywords: Longitudinal Stability; Computational Fluid Dynamics (CFD); Aerodynamics; Wing-Strake; Vortex Flow

Abstract

Changes in flight stability characteristics at the advanced stage of aircraft design are complex and require thorough investigations. This paper examines the impact of wing strake modification on high-performance aircraft using computational fluid dynamics (CFD). The dynamic behaviour is calculated using the forced oscillation technique, while the effect of geometric variation on longitudinal stability characteristics is extensively studied. Steady-state experimental data is utilised to validate the computational setup. Static aerodynamic coefficients, dynamic stability derivatives and the positions of aerodynamic and pressure centres are employed to quantify the changes. Furthermore, the alterations in stability characteristics are correlated with flow physics. The results indicate a reduction in longitudinal static and dynamic stability at various flight conditions due to the proposed modification. This deliberate reduction was necessary to accommodate the installation of a fly-by-wire system. The discussed design changes have been effectively implemented on an in-service aircraft.

Nomenclature

M	moment
L	lift
D	drag
q	pitch rate
p	roll rate
r	yaw rate
y^+	dimensionless distance for first cell
V_∞	free stream velocity
q_∞	dynamic pressure
V_H	horizontal tail volume ratio
l_t	distance from horizontal tail to CG
$\bar{C}$	chord length
K_q	reduced pitch rate
K	reduced frequency
S	wing area
MAC	mean aerodynamic chord
C_D	drag coefficient
C_L	lift coefficient
C_M	moment coefficient
$C_{M_q} + C_{M_{\dot{\alpha}}}$	moment damping coefficient

$C_{L_q} + C_{L_{\dot{\alpha}}}$	lift damping coefficient
Δt	time step
f	oscillation frequency

Greek symbol

α	angle-of-attack
$\dot{\alpha}$	rate of change of angle-of-attack
β	sideslip angle
ρ	density
ϵ	wing downwash
ω	oscillation velocity

1.0 Introduction

Changes in aircraft configuration in the design, development and up-gradation are commonplace in the aerospace industry. Prototype evaluations should be conducted as soon as possible during the design phase to save time, money and other resources. Verifying each new design quickly, inexpensively and safely is essential. Historically, prototypes were developed for new aircraft designs before they were tested. The entire manufacturing process and time are wasted if the prototype performs poorly. The problem of testing prototypes was solved through empirical and numerical techniques in the past. However, both were flawed by the need for more accuracy. In addition to saving a lot of money and manufacturing hours, these empirical and numerical methods could be more accurate in determining an aircraft's actual behaviour. Computational fluid dynamics (CFD) is the method that can accurately predict the fluid behaviour of an aircraft. Furthermore, this method is cost-effective and takes relatively little time to develop a new aircraft model.

Historically, Bryan introduced the notion of stability or aerodynamic derivatives in 1911 [1]. Based on Nguyen's study [2], dynamic derivatives of the aerodynamic model significantly affected the stability characteristics of aircraft at high angles of attack and rates. The investigation of unsteady aerodynamics effects on aircraft motion was done first by Jones and Fehlner [3] and dynamic stability derivatives of the SDM under forced oscillation to find a proper experimental setup for a generic combat fighter performed by Mehmet [4].

Dynamic stability coefficients in the past were occasionally assumed to be negligible or computed as a small constant based on simple approximations of the static stability coefficients [5]. Increasing complexity in modern designs and extreme flight conditions increase the importance of stable dynamic characteristics. Especially for slender vehicles with fins, the damping derivatives significantly affect the vehicle's ability to respond at high speed and extremely high angle-of-attack [6]. Since Apollo and Viking programs, predicting dynamic stability derivative has been challenging [7].

For the prediction of dynamic derivatives, the time-dependent motion must be able to compute the aerodynamic response, which excites the applicable aerodynamics. Computing higher-order stability derivatives for general configurations and flow conditions is computationally challenging, as it involves simulating an unsteady flow of a moving geometry. Therefore, dynamic stability derivatives are calculated only at a few critical points using CFD or restrictive approximation methods and then extrapolated to cover the desired range. The traditional technique of predicting dynamic derivatives, such as wind tunnel testing, is expensive and complex. As aircraft designs continue to evolve, they become more manoeuverable. Stability and control laws for an aircraft must be developed using a high-fidelity aerodynamic database of dynamic derivatives.

For fighter aircraft, it is essential to have highly manoeuverable capabilities, and a stable aircraft cannot do that. In all the discussions of vortex flows and induced lift, stability characteristics change with the effect of the wing strake. A wing strake aligns the vortex flow, and its vortex combined with the wing vortex creates a strong vortex which, at a high angle-of-attack, leaves the surface of the wing

https://doi.org/10.1017/aer.2024.32 Published online by Cambridge University Press

early and leaves a high-pressure region below the vortex on the surface of the wing, which pushes the wing down and reduce the stability.

Many hybrid wing planforms have been studied with the idea of using them on supersonic transports or combatants. Initially, wind tunnels and flight tests did the work on wing strake. Planform areas were developed for use on supersonic fighters. Several fighter aircraft, including the F-16 and F-18, have planform areas to improve flight performance. F-16 and F/A-18 aircraft have wing strakes that cause vortex lift. The vortex lift occurs when captured vortices are generated from the sharply swept leading edge of the wing. Although flow separating from the surface causes a decrease in the lift, due to the induced lift effect, an extra lift is generated.

Morton [8] did a CFD analysis of F-16 aircraft. F-16 aircraft has a strake body, which induces instability at the subsonic regime. A similar effect was observed for F-18 aircraft, but with experimental analysis [9]. Although a small amount of research is available on the wing-strake aircraft's stability, much research is done on the aerodynamics of wing-strake alone. Most of this research is performed with the wing-strake arrangement on delta wings; one example is the work of Fujii [10], but there are no stability calculations.

Lamar visited stability characteristics of wing-strake arrangements [11] in 1980; he used 16 analytically and empirically designed strakes. This efficiency analysis shows that using a leading-edge sweep greater than 44^{o} gives the extra lift. Luckring [12] shows that reducing leading-edge suction results in delayed and smeared separation. This efficiency analysis also explains that increasing the wing area is not as effective as adding a wing strake; a wing strake also causes an increase in drag but not as much as it increases lift, which makes it a better choice than other lifting surfaces like canards.

The effect of wing-strake on a generic aircraft configuration was evaluated in [13], but stability characteristics were not visited. CFD aerodynamic analysis of different strake configurations was performed in [14]. Also, a lot of research on stability characteristics of aircraft is present in literature but only on the standard dynamic model (SDM) like the work of Mehmet [4] through experimental forced oscillations, and Ronch [15] through CFD is present.

Stability calculations through CFD on wing-strake arrangements are done by Carter [16], in which many shapes of delta wings and strake configurations were compared in regards to their stability characteristics. Carter [16] analysed the stability characteristics of 12 configurations of 5^{th} generation delta wings. It was concluded that adding a wing strake decreases the longitudinal stability of the aircraft.

Many aircraft use different strakes for various purposes, such as the Concorde SST's nose strake forward to the fuselage to control fuselage flow at high angles of attack [17].

In conclusion, for many reasons, stability calculation through CFD on wing-strake arrangement incorporated on any specific aircraft body is a missing link in the literature.

2.0 Problem formulation

When the aircraft under consideration goes through a flight testing phase, it develops a need for design improvement in two areas: supersonic drag reduction and pushing the aircraft's aerodynamic centre forward to take full advantage of the digital fly-by-wire flight control system's capacity. For this refinement, wing-strake or leading-edge extension is the best way forward.

It is improbable that any stability or aerodynamic calculation on the concerned aircraft is available. But, in 2007, [18] provided insight into the aerodynamic advantages of wing-strake arrangement on the aircraft model used in this study using the high-order panel method; however, dynamic behaviour was absent. Dynamic behaviour of spin characteristics, yawing moments with elevator deflection, and asymmetric behaviour using CFD were evaluated of this aircraft in 2016 by Masud et al. [19]; moreover, the high angle-of-attack dynamics, yaw and pitch behaviour were also considered. Recently, in 2021, [20] longitudinal steady state and 1 DOF forced pitch-up analysis was done through CFD analysis, which gave this research its validation study.

https://doi.org/10.1017/aer.2024.32 Published online by Cambridge University Press

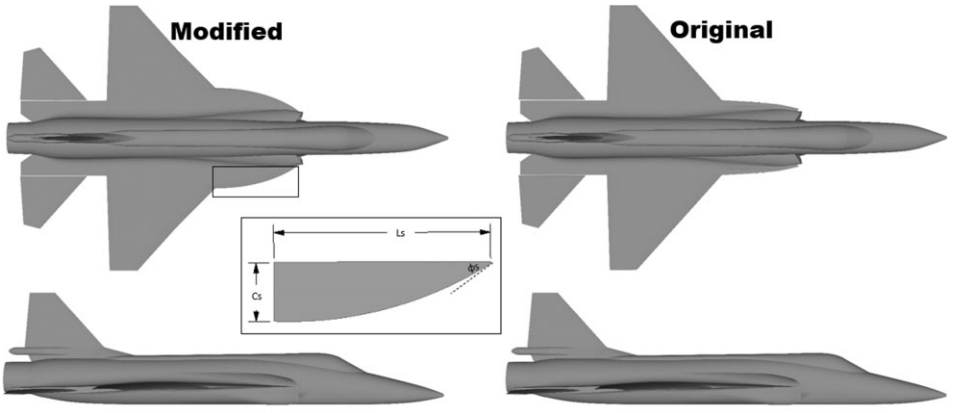

Aircraft Configuration	Original	Modified
Strake Total Area (As)	1.2 m²	2.33 m²
Strake Length (Ls)	2.52 m	2.67 m
Strake Sweep Angle (ϕs)	15°	36°
Strake Chord Length (Cs)	0.35 m	0.77 m
Mean Aerodynamic Chord	2.445 m	
Span	8.488 m	
Reference Area	24.5	

Figure 1. *Aircraft geometry and description. Left modified and right original.*

The wing-strake arrangement used in this work is a modified aircraft prototype. A comparison analysis was done with an original aircraft prototype to identify the effect of wing-strake arrangement on flight stability.

Therefore, this study aims to perform comparative stability and aerodynamic analysis. Furthermore, this study aims to analyse the impact of the wing-strake arrangement on the longitudinal stability of the aircraft and explore the aerodynamic advantages resulting from this modification. Since precise information regarding the centre of gravity (CG) for the given aircraft is not available, the analysis was conducted based on an estimated location of CG. While this assumption may not provide the exact information on the aircraft's longitudinal stability coefficients, it does provide valuable insight into the effect of the wing-strake arrangement.

2.1 Geometric description

The geometric modeling of two models for CFD simulations was made using ®. In the modified geometry, a more extensive strake configuration was added. The original geometry, which has a smaller strake configuration, was also modeled. The parameters used to describe strake geometry are strake length (Ls), strake sweep angle (ϕs), strake total area (As), and strake chord length (Cs).

In the absence of precise CG information pertaining to the aircraft in question, it becomes necessary to employ an educated estimation regarding the CG's probable placement. The centre point for both prototypes is chosen to be at X/L_x=0.6143, Y/L_y=0, Z/L_z=0 (for reference, see Fig. 8). The details of geometries are in Fig. 1.

After completing the geometric modeling, setting the case for CFD analysis is essential. To do that, a spherical domain was created outside the aircraft model. By keeping the domain solid and hollowing out the aircraft model.

In this study, both static and dynamic stability are emphasised. An outer rectangular domain was created with a spherical domain inside to allow aircraft to move in the spherical domain, using the sliding mesh technique.

https://doi.org/10.1017/aer.2024.32 Published online by Cambridge University Press

Table 1. *Grid details of both aircraft's configurations*

Parameters	Modified	Original
No. of elements	28,291,641	24,463,653
No. of nodes	8,866,474	7,634,508
No. of layers (prism)	15	15

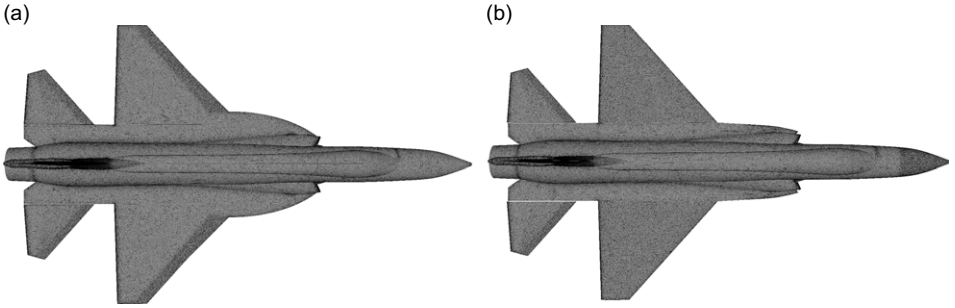

Figure 2. *Surface mesh of modified and original configuration.*

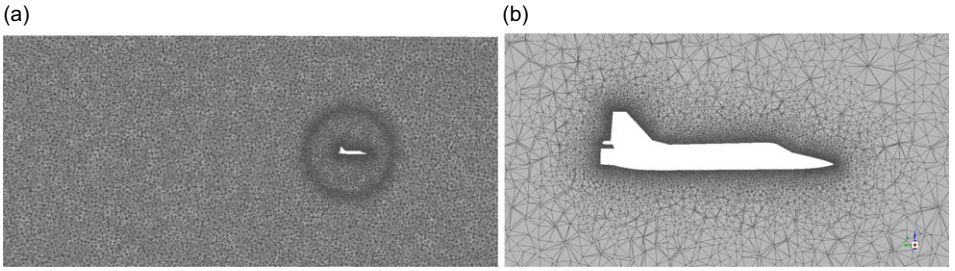

Figure 3. *Unstructured grid for inner and outer domains.*

The meshing of geometry is an integral part of CFD calculations. A better mesh will ultimately yield accurate stability derivatives. The best way to mesh complex geometries is to divide the geometry into parts to facilitate meshing complex curves and surfaces. An unstructured grid was made with tetrahedral elements. The grid details are illustrated in Table 1. In addition, prism mesh was formed near the surface. The mesh was resolved in the modified configuration using the same settings as the original; the slight difference in the surface mesh is because the modified model has a strake configuration, shown in Fig. 2. Also, the inner and outer domain mesh is shown in Fig. 3.

2.2 Computational setup for validation studies

To validate the wing strake configuration (modified), experimental results were compared with those obtained through CFD. The experimental results mentioned in [20] are conducted at Mach number 0.6, with the moment coefficient calculated at the aircraft's mass centre, which is about: $X/L_x = 0.6$, $Y/L_y = 0$, $Z/L_z = 0$ (for reference see the Fig. 8) in [20]. For a rigorous validation of the computational fluid dynamics (CFD) findings, the centre point of the modified configuration was intentionally repositioned

https://doi.org/10.1017/aer.2024.32 Published online by Cambridge University Press

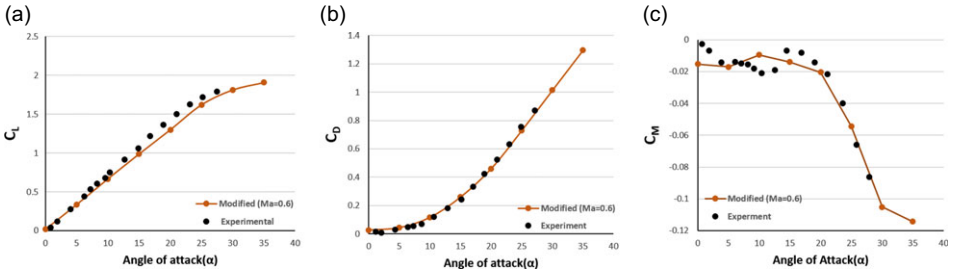

Figure 4. *Validation of modified configuration's static state results with experimental.*

to $X/L_x = 0.6, Y/L_y = 0, Z/L_z = 0$. This deliberate shift in the centre point allowed for a direct comparison between the static CFD results of the modified configuration at Ma = 0.6 and the corresponding experimental results (Fig. 4).

The results showed that the CFD results corresponssd greatly with the experimental results. The most important parameter for stability studies is the moment coefficient, which closely resembles the experimental results at a low angle-of-attack. This discrepancy could be due to the potential influence of uncertainties in experimental data, as exact information regarding the experimental setup is unknown.

Still, as the angle-of-attack increases, the results correspond almost precisely. The results of the coefficient of lift and coefficient of drag corresponded almost precisely. This means that the CFD setup is accurate enough to determine the stability characteristics of the aircraft.

The validation study determined that the turbulence model best predicts the stability characteristics with experimental studies is the Spalart Allmaras (SA) model.

2.3 Computational solver setup for static state analysis

For static CFD analysis of an aircraft, Ansys Fluent needs subsonic and supersonic flow conditions defined in Table 2.

Pressure far-field boundary condition was applied at the outer domain. The pressure-based solver was used for the subsonic flow regime, and the density-based solver was used for the supersonic. The converged results determine the aerodynamic and longitudinal static stability characteristic of the aircraft.

Due to the supersonic regime, a time-dependent simulation must be performed to incorporate that unsteadiness.

2.4 Computational solver setup for dynamic analysis

For dynamic analysis, forced oscillations were performed using the sliding mesh technique. Equations 1–3 calculated the parameters used for these calculations. These conditions allowed the aircraft to oscillate about its centre as the solver calculated the coefficient of the moment and lift in the form of sinusoidal curves. The parameters are given in Table 3 for Mach = 0.6, 1.4:

$$f = \frac{V_\infty k}{\pi d} \tag{1}$$

$$k = \frac{\omega d}{2V_\infty} \tag{2}$$

$$\Delta t = \frac{\pi d}{N V_\infty k} \tag{3}$$

https://doi.org/10.1017/aer.2024.32 Published online by Cambridge University Press

Table 2. *Subsonic and supersonic boundary conditions attributes for three different Mach numbers*

Parameters	Subsonic	Supersonic
Mach numbers	0.15 and 0.6	1.4
Pressure	101,325 Pa	101,325 Pa
Temperature	288 K	288 K
Turbulence model	Spalart Allmaras	Spalart Allmaras
Time step size (Δt)		0.002 s

Table 3. *Dynamic calculation parameters*

Parameters	Subsonic	Supersonic
Mach number	0.6	1.4
Time step size (Δt)	0.0044 s	0.00188 s
Reduced frequency (k)	0.0855	0.0855
Oscillation frequency (f)	2.27 Hz	5.3 Hz
Oscillation amplitude	5^o	5^o

Where N = number of time steps (Δt) for one oscillation, k is the reduced frequency, d is characteristic length and f is the oscillation frequency. The value of k determines the degree of instability in a system. If a system is highly unsteady and we use a low value of k to calculate dynamic stability, getting a converged solution would take a lot of time. So, it is essential to calculate the value of k specific to the system under harmonic motion.

The convergence of dynamic simulation is checked by analysing the sinusoidal curves of the coefficients. For longitudinal stability, the sinusoidal curves of the coefficient of the moment will be observed.

3.0 Results and discussion

3.1 Impact of static aerodynamic coefficients on aircraft's stability

For longitudinal stability analysis, static CFD comparison of the coefficients C_L, C_D, and C_M will evaluate the aerodynamics and stability characteristics for both aircraft configurations (original and modified).

For Ma = 0.15, at around 25^o AOA, the lift coefficient increases for modified and the maximum lift increases by 5.728%. For Ma = 0.6, the increase in lift begins at 20^o AOA, with a 6.0358% increase in maximum lift. For Ma = 1.4, the increase in lift coefficient begins at around 10^o AOA, with only a 2.8998% increase in maximum lift (see Fig. 5). Adding a strake to the aircraft generally increases lift, consistent with the literature review.

The drag coefficient at Ma = 0.15, there is an increase in drag coefficient observed at 20^o for modified.

At Ma = 0.6, there is an increase in drag coefficient observed at 15^o AOA for modified, and finally, at Ma = 1.4, there is an increase in drag coefficient for modified configuration and starts at 15^o (See Fig. 6).

For C_M at Ma = 0.15, there is stability observed for original until 25^o AOA; then there is slightly less stability until 30^o AOA. Looking at the modified curve, instability is observed until 25^o AOA, and then there is slight stability until 30^o AOA, and then it becomes unstable again.

For Ma = 0.6, the original configuration is stable, but the modified configuration is unstable until 20^o AOA and then stable afterward.

With an estimated CG location, it is observed that the instability in the modified configuration is primarily due to this CG shift. This relationship is evident in Fig. 4c's CM validation curve, where adjusting the CG point shifted the modified configuration from instability to static stability. These

https://doi.org/10.1017/aer.2024.32 Published online by Cambridge University Press

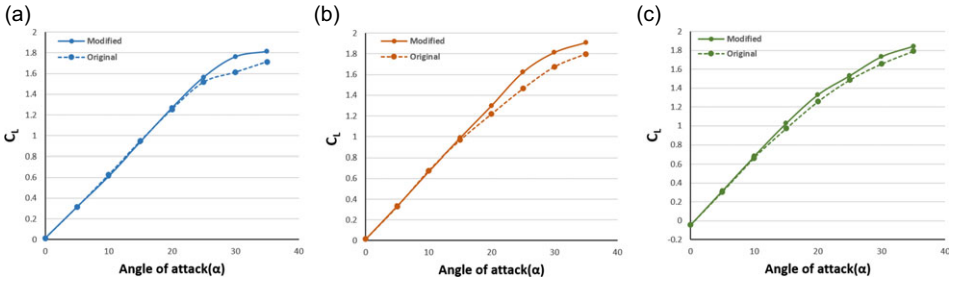

Figure 5. *Lift coefficient for original and modified at different Mach numbers with a variation of the angle-of-attack.*

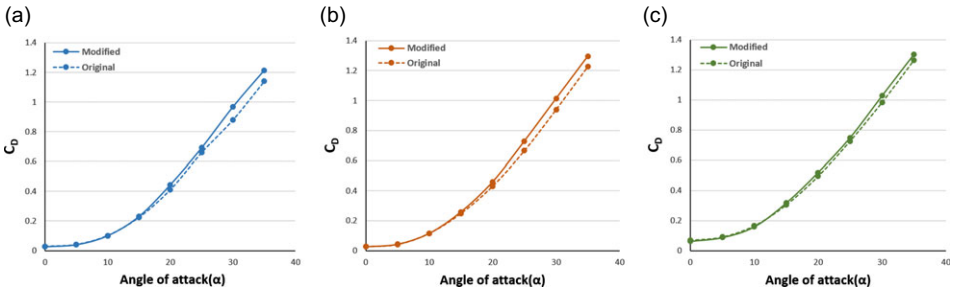

Figure 6. *Drag coefficient for original and modified at different Mach numbers with a variation of the angle-of-attack.*

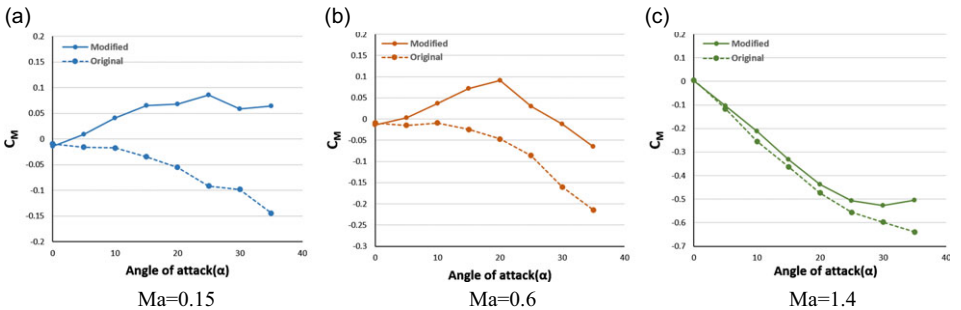

Figure 7. *Moment coefficient for original and modified at different Mach numbers with the variation of the angle-of-attack.*

results emphasise the CG's role in aircraft stability, especially in modified designs like the wing-strake arrangement.

Finally, for Ma = 1.4, both modified and original configurations show stability until 30^o AOA, modified shows slight instability after 30^o AOA (See Fig. 7).

So, adding a strake causes instability in aircraft.

https://doi.org/10.1017/aer.2024.32 Published online by Cambridge University Press

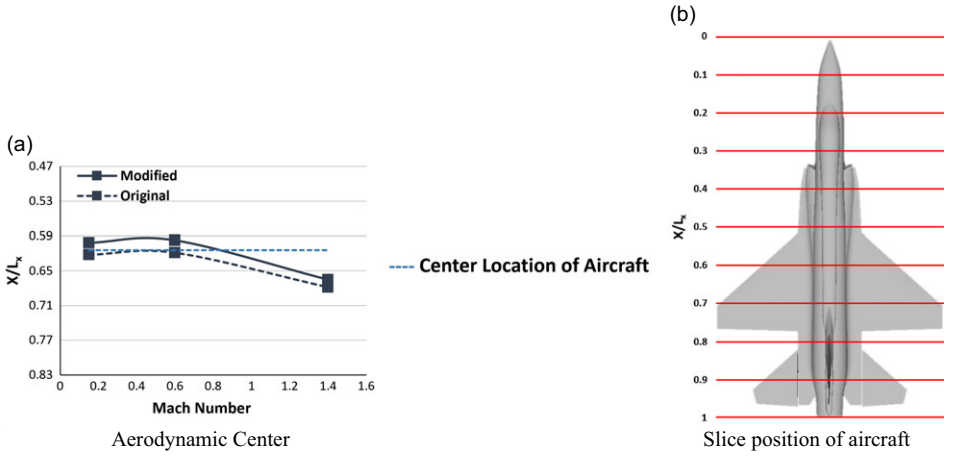

Figure 8. *Aerodynamic centre position of aircraft and slice positions of aircraft.*

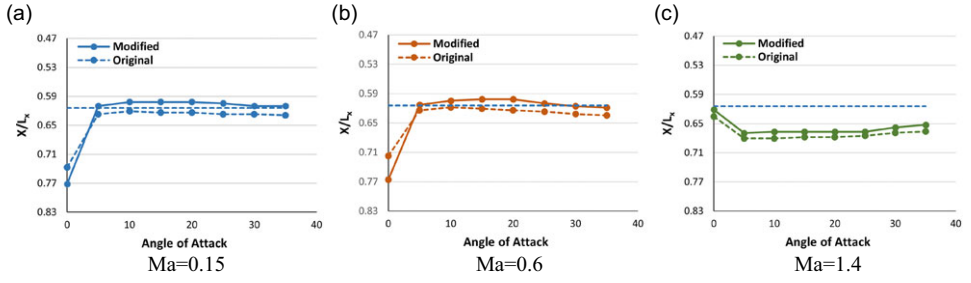

Figure 9. *Centre of pressure position of aircraft.*

3.2 Aerodynamic centre and centre of pressure

The point of constant pitching moment or aerodynamic centre (Fig. 8a) and the point of concentration of all forces or the centre of pressure (Fig. 9) moves aft of the aircraft when the aircraft is in supersonic regime. This means that at the supersonic regime, both aircraft configurations are longitudinally stable, the slight forward shift for modified configuration from the centre point ($X/L_x = 0.6143$ in Fig. 8b) at subsonic regime indicates loss in stability.

3.3 Flow physics of aircraft in static state

Comparing the flow behaviour at different flight conditions together with coefficient curves can better explain the aerodynamic and stability characteristics of aircraft, and a better conclusion can be drawn on the difference in flight behaviour of both aircraft models.

Note that only those angles of attack will be considered, which shows some significant differences in the flow behaviour of both aircraft models. Two types of visualisation techniques are used for static analysis.

1. A significantly high angle-of-attack case for both aircraft models are compared side by side with scales for length and half span of aircraft (Figs. 10 and 12). Half of the original configuration is at the left of the scale, and half of the modified configuration is at the right of the scale.

https://doi.org/10.1017/aer.2024.32 Published online by Cambridge University Press

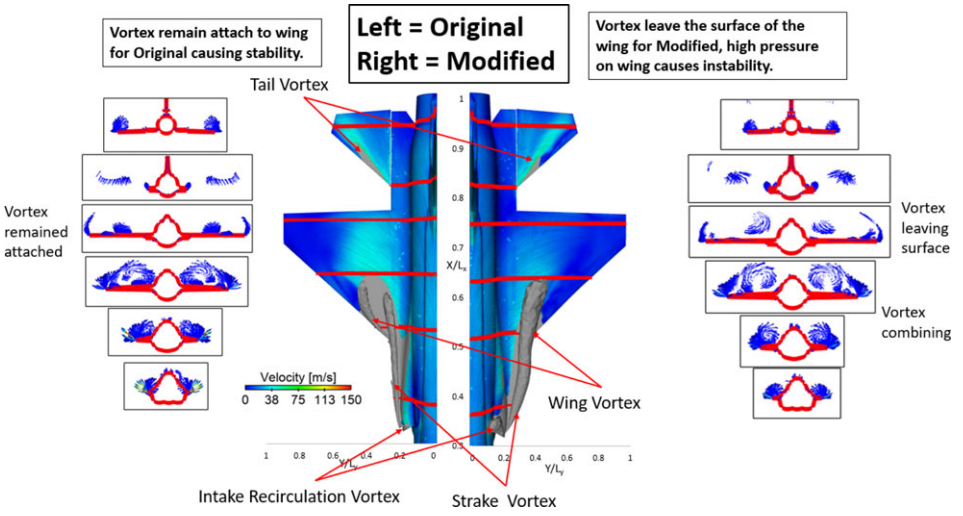

Figure 10. *Flow visualisation at Mach = 0.15 and $\alpha = 30^o$. Left is original, and right is modified.*

- To gain deeper insights into flow attachment and detachment on aircraft, the velocity flow field at a surface offset of -0.0001m was analysed. This approach provides a clearer depiction of shear layer dynamics and boundary layer behaviour, making it particularly advantageous for identifying the onset of flow separation and understanding the extent of attached flow regions. Additionally, this offset velocity contour directly visualises the flow field, capturing velocity fluctuations near the surface and detecting subtle changes in the flow pattern. Although static pressure provides good insights into pressure distribution on the surface, these advantages may not be as apparent in static pressure contours on the surface because, under certain conditions, static pressure contours on the surface may mask localised flow features due to their sensitivity to pressure gradients.
- A total pressure iso-surface is created to visualise the vortex clouds.
- At different sliced aircraft planes, the vector field of Q-criterion was shown to analyse the vortices' attachments and detachments and the location of vortex breakdown.

2. To analyse the effect of the angle-of-attack on the coefficient of the moment (Figs. 11 and 13).

- Total pressure iso surface is compared side by side on half of both aircraft models to visualise the formation of vortex clouds.
- Velocity flow field at -0.0001m offset of the surface.

3.3.1 Mach 0.15

For the Mach 0.15 case, at 30^o AOA, the strake vortex is stronger than the wing vortex for modified due to low speed. The wing vortex immediately combines with the strake vortex to form a stronger vortex, and this strong vortex detaches from the surface at $X/L_x \simeq 0.68$ (right side of Fig. 10).

The original configuration wing and strake vortices are almost the same strength. They combine shortly after formation at $X/L_x \simeq 0.65$ but are not as strong as modified. Unlike modified, this vortex remains attached to the wing surface (left part of Fig. 10) and breaks down at around $X/L_x \simeq 0.8$ away from the wing surface.

In Fig. 11b, the high-velocity region (green region indicating attached flow) slowly approaches the fuselage. Eventually, it vanishes from the wing as the angle-of-attack increases of the modified configuration. A greater vortex-induced lift occurs at high α due to the powerful vortices (Fig. 11a).

https://doi.org/10.1017/aer.2024.32 Published online by Cambridge University Press

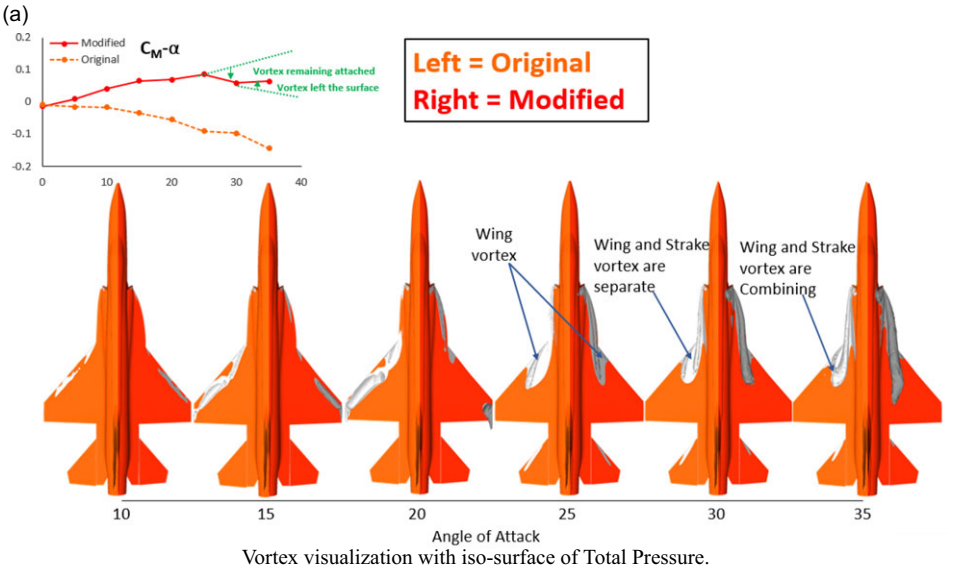

Vortex visualization with iso-surface of Total Pressure.

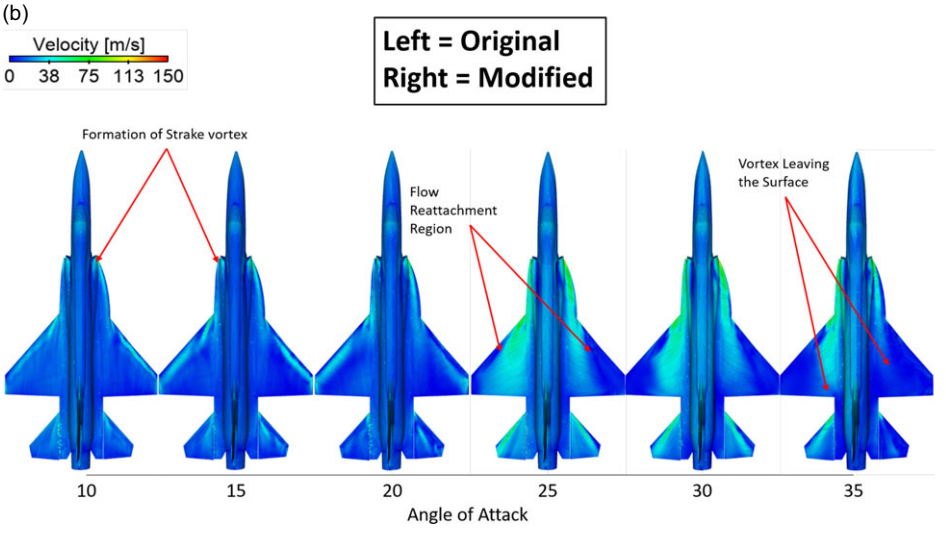

Flow visualization with velocity at (-0.0001 m) offset of the surface.

Figure 11. *Flow visualisation at Ma = 0.15.*

The leading-edge vortices increase suction on the surface of the wing strake and wing. This suction delays the stall, so a strong vortex or a higher induced suction will result in a higher lift coefficient [21].

Additionally, the vortex breakdown at the rear part of the wing (aft of moment reference point) of the modified configuration, which slowly increases as the angle-of-attack increases (blue region indicating detached flow), decreases the induced suction. This leads to a loss in vortex lift [13] and can generate some downforce. Conclusively, the strong vortices dominantly increase the lift coefficient, eventually raising C_{Lmax} (Fig. 5a).

Also, this vortex lift at the front part of the aircraft (forward of moment reference point) and downforce at the rear part may cause additional pitch moment, resulting in plausible instability of the modified configuration.

https://doi.org/10.1017/aer.2024.32 Published online by Cambridge University Press

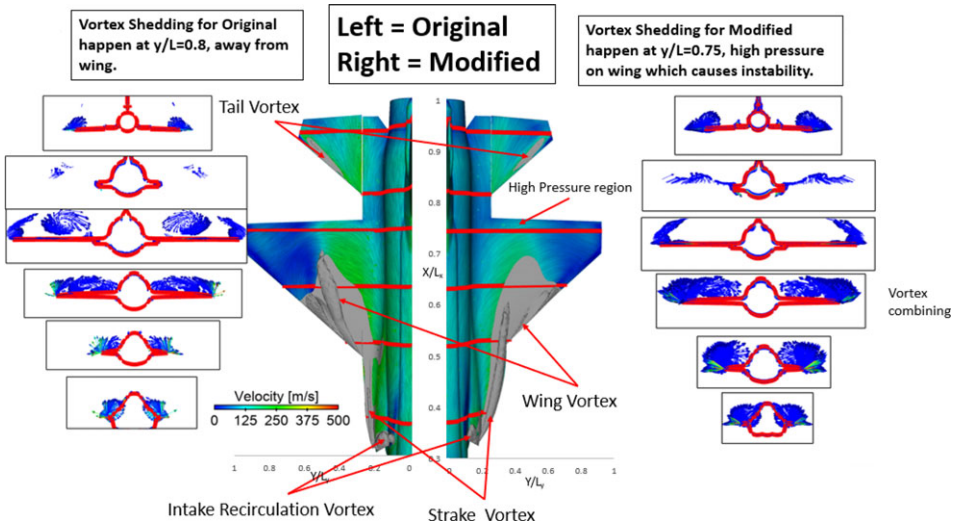

Figure 12. *Flow visualisation at Mach = 0.6 and $\alpha = 20^o$. Left is original, and right is modified.*

For the original, the attachment/reattachment line (transition region of green and blue in Fig. 11b) moves towards the fuselage. The flow remains majorly attached to the wing surface, which indicates that this configuration is likely to be more stable than the modified. Wing and strake vortex for original are separate at low α or even at high α; they combine at above 30^o AOA as shown in Fig. 11a, which explains why original is unable to produce more lift at high α.

3.3.2 Mach 0.6

For the case of Mach 0.6, at 20^o AOA, wing and strake vortices are separate and not very strong for original, but the flow remains attached to the surface (green region of the left side of Fig. 12). The vortices are shed after the wing at around $X/L_x \simeq 0.8$.

For modified (right side of the Fig. 12), the vortex of the strake is strong. The wing vortex is weak, so it does not increase the strength of the strake vortex much, which eventually dies down at $X/L_x \simeq 0.75$ above the wing surface, which may cause an induced pitch moment that can cause static instability.

At low angles of attack, the vortex remains attached to the wing's surface with a strake vortex combined with the wing vortex. At 15^o AOA, vortex shedding occurred at the top of the wing, resulting in an additional pitch-up moment indicating plausible instability at low α.

After 20^o, the AOA vortex becomes stronger and remains attached to the wing surface, which causes an extra vortex lift on the wing. Vortex shedding moves away from the wing's trailing edge will cause the aircraft to become stable at high α (Fig. 13a and 13b).

For original, weaker vortices are formed at a low angle-of-attack; the small strake causes a vortex at 15^o AOA. At 20^o AOA (Fig. 12), wing and strake vortices separate and then begin to combine after 25^o AOA. The vortex breakdown does not occur at the top of the wing surface, and flow remains attached to the wings. Also, the vortex strength is lower than modified, and the reattachment/detachment line moves closer to the fuselage as the angle-of-attack increases. Contrary to that, the reattachment/detachment line moves away from the fuselage for modified, meaning more potential and vortex lift (Fig. 13b).

3.3.3 Mach 1.4

For Mach 1.4, both aircraft configurations are statically stable because the induced vortex effect increases at the static state and supersonic speed. The flow remains majorly attached to the body (Fig. 14).

https://doi.org/10.1017/aer.2024.32 Published online by Cambridge University Press

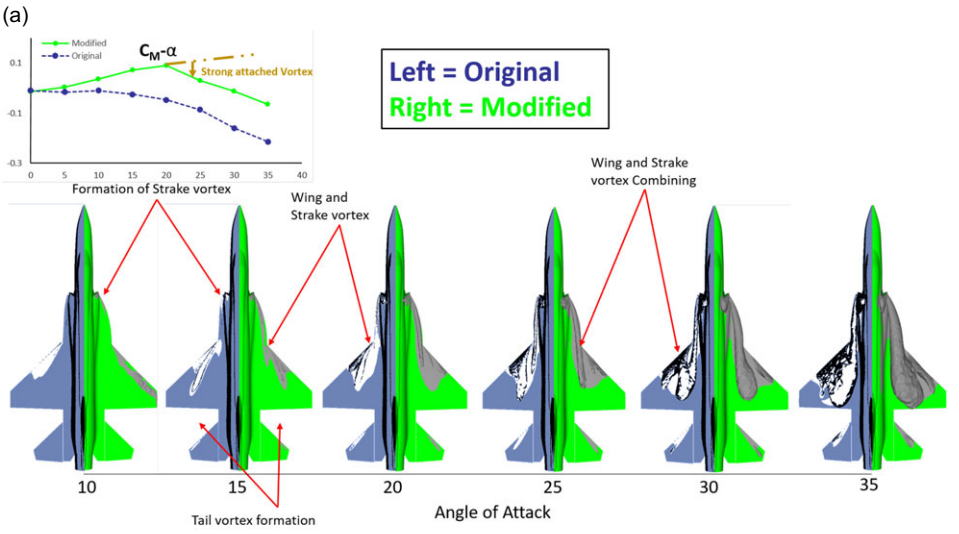

Vortex visualization with iso-surface of Total Pressure.

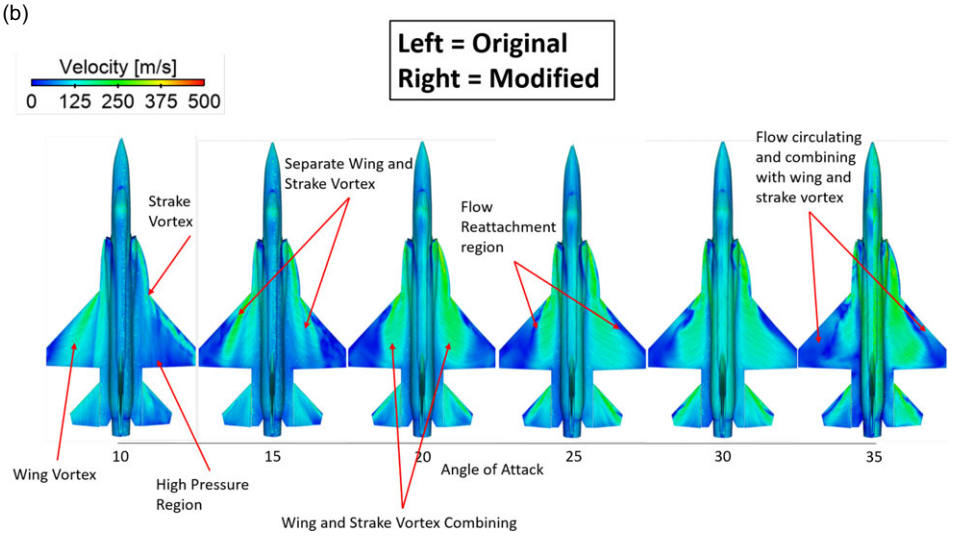

Flow visualization with velocity at (-0.0001 m) offset of the surface.

Figure 13. *Flow visualisation at $Ma = 0.6$.*

As previously discussed, flow attachment is a significant cause of stability. Also, a shock wave's effect may cause instability, but the shock wave effect is not as significant for this particular aircraft to cause instability in a static state.

Looking at the velocity distribution on the offset surface. At low α, flow is attached to the surface. Still, at 10^o AOA flow starts to leave the surface for the modified configuration but not for the original (See Fig. 14), which explains why the modified configuration is slightly less stable than the original, which Fig. 5 indicate that start from 10^o AOA.

3.4 Impact of dynamic aerodynamic coefficients on aircraft's stability

The longitudinal dynamic behaviour of an aircraft is usually evaluated with the combined derivative $C_{M_q} + C_{M_{\dot{\alpha}}}$ and $C_{L_q} + C_{L_{\dot{\alpha}}}$ under different flight conditions and frequency of oscillation of $\Delta\alpha = 5^o$.

https://doi.org/10.1017/aer.2024.32 Published online by Cambridge University Press

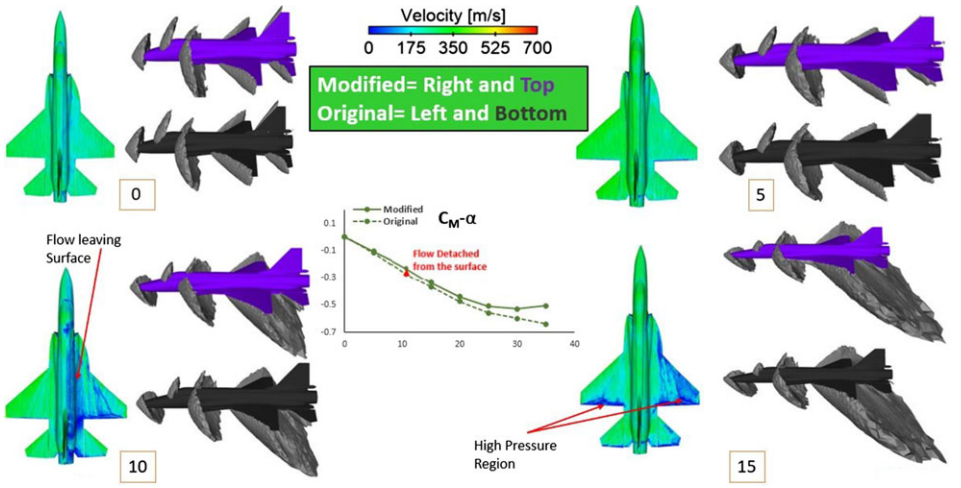

Figure 14. *Flow visualisation at Mach = 1.4. The left part of the velocity flow on the aircraft and the bottom shock wave representation is original, and the right part of the velocity flow on the aircraft and top shock wave representation is modified.*

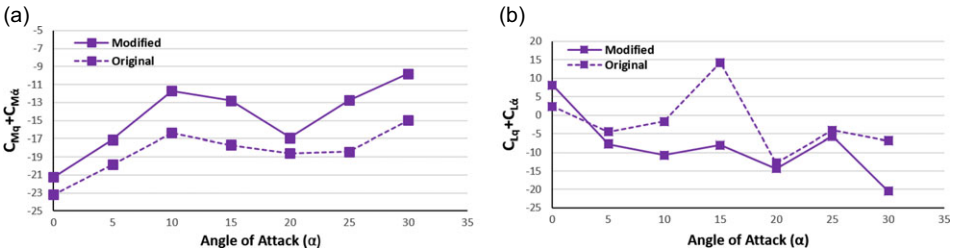

($C_{M_q} + C_{M_{\dot{\alpha}}}$) versus angle of attack α.

($C_{L_q} + C_{L_{\dot{\alpha}}}$) versus angle of attack α.

Figure 15. *Damping coefficients at Ma = 0.6.*

This study conducts a comparative analysis with damping derivatives for modified and original configurations at subsonic and supersonic regimes. It also uses different parameters like reduced frequency and Mach number to identify their effect on the dynamic behaviour.

Mach 0.6 is treated as the subsonic Mach number to identify the subsonic dynamic behaviour of both aircraft configurations. Table 3 gives the parameters used for this study.

The plot of $C_{M_q} + C_{M_{\dot{\alpha}}}$ vs α shows that at low angles of attack, both configurations exhibit stability, and at high angles of attack both configurations show less stability. Generally, the original configuration is more dynamically stable than the modified at different angles of attack at this particular reduced frequency and oscillatory amplitude (see Fig. 15a).

The behaviour of $C_{L_q} + C_{L_{\dot{\alpha}}}$ at the same Mach number in Fig. 15b indicates that the modified configuration has a more negative damping lift coefficient. It is because vortex-induced flows are present in modified due to a strake, which causes it to delay the response and takes more time to reach a particular lift value at a particular angle-of-attack.

Ma = 1.4 is used for supersonic analysis for the longitudinal dynamic behaviour of the aircraft configurations. The value of reduced frequency is kept constant for comparison, and other parameters are calculated using this Mach number (Table 3).

While it is not ideal for the aircraft to move at supersonic speed and oscillate at a high angle-of-attack, dynamic derivatives at high α are calculated for comparison with the subsonic flow.

https://doi.org/10.1017/aer.2024.32 Published online by Cambridge University Press

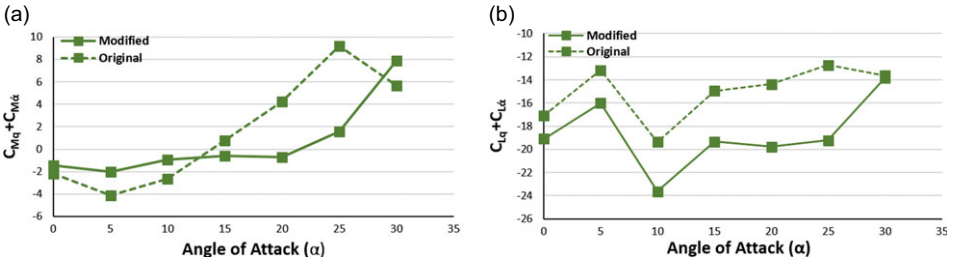

$(C_{M_q} + C_{M_{\dot{\alpha}}})$ versus angle of attack α. $(C_{L_q} + C_{L_{\dot{\alpha}}})$ versus angle of attack α.

Figure 16. *Damping coefficients at Ma = 1.4.*

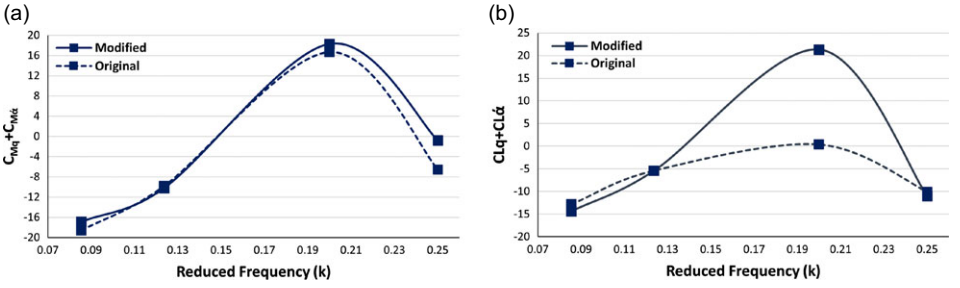

$(C_{M_q} + C_{M_{\dot{\alpha}}})$ versus Reduced Frequency $(C_{L_q} + C_{L_{\dot{\alpha}}})$ versus Reduced Frequency

Figure 17. *Damping derivatives with reduced frequency variation. At Ma = 0.6 and α = 20°.*

First, $C_{M_q} + C_{M_{\dot{\alpha}}}$ observed in the Fig. 16a shows that the original configuration is more dynamically stable than modified at low angles of attack, similar to the behaviour observed at Ma = 0.6. But the state reverses at 15° AOA where modified becomes unstable, but original is still dynamically stable and becomes unstable at 25° AOA. The damping coefficient values indicate less stability for both aircraft configurations at supersonic speed than subsonic speed at this reduced frequency.

The damping lift coefficient's behaviour is similar for Ma = 1.4 (Fig. 16b) and Ma = 0.6 with few discrepancies.

3.5 Parametric analysis on dynamic damping derivatives

It is an acceptable approach to explain the parametric changes of aircraft's dynamic behaviour side by side for better understanding. First, the reduced frequency's effect at Ma = 0.6 and $\alpha = 20^o$ of both configurations are analysed. Both configurations have similar damping coefficients at lower reduced frequencies with negative signs, indicating stability. However, at a reduced frequency of 0.2, a noteworthy deviation occurs where both configurations transition into an unstable state with positive damping coefficient values. However, the modified configuration exhibits slightly greater instability (Fig. 17a). This behaviour can be attributed to the aircraft's inherent unsteadiness, which can cause a sudden loss of stability. The strake-enhanced geometry is contributing slightly more to this effect.

Reduced frequency is proportional to the frequency of motion and the characteristic length divided by the free stream air speed ($k = \omega c/V$). It characterises the unsteadiness of the flow experienced by the aircraft. A lower reduced frequency value is associated with greater dynamic stability, depicting smoother and more predictable motion. Conversely, a higher value indicates a higher likelihood of dynamic stability, potentially leading to less predictable and more oscillatory behaviour.

https://doi.org/10.1017/aer.2024.32 Published online by Cambridge University Press

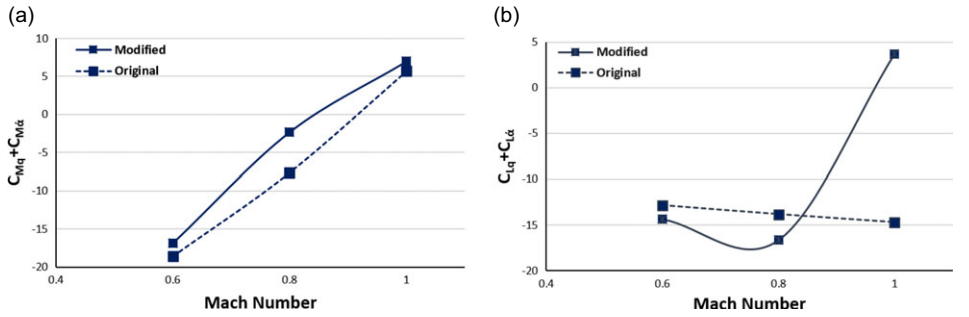

$(C_{M_q} + C_{M_{\dot{\alpha}}})$ versus Mach number $(C_{L_q} + C_{L_{\dot{\alpha}}})$ versus Mach number

Figure 18. *Damping derivatives with mach number variation. At* $\alpha = 20^o$.

The value of reduced frequency 0.2 acts as a critical value. Beyond that at a reduced frequency of 0.25, both configurations again exhibit stability, albeit the modified configuration remains less stable than the original.

For lift damping, there is a slight difference in the behaviour. The lift damping shows similar abnormality at $k = 0.2$ for modified as pitch damping (Fig. 17b). This abnormality is not very significant in the original.

Now, consider the Mach variation curves calculated at a reduced frequency of 0.0855. Figure 18a shows high instability at transonic speeds. Comparing the values of moment damping coefficients at Figs. 15a and 16a, the aircraft should be dynamically stable at supersonic speeds.

With the change in Mach number, lift damping slightly increases until Ma = 1.0 for the original configuration (Fig. 18b). For the modified, there is a drastic reduction in lift damping at the transonic regime.

3.6 Flow behaviour with forced oscillations

With forced oscillation, the oscillatory motion perturbs the flow passing over an aircraft. To explain this effect, consider the flow condition of $\alpha = 30^o$ and Ma = 0.6 (Fig. 19). These figures visualise vortex flow above the aircraft surface using the total pressure iso-surface. The right part of the figure shows modified's flow behaviour, and the left side shows original's flow behaviour. In this figure, the vortex behaviour at different aircraft positions is formed using the Q-criterion and visualised with vectors. These positions are X/L_x=[0.35, 0.5, 0.62, 0.73, 0.82, 0.98]. There is a pitch-up motion from Fig. 19a–19c, and a pitch-down motion is from Fig. 19–19e.

The flow on the aircraft's surface and the vortex flow on top of the surface is an excellent way to explain the flow behaviour. The flow on the -0.0001m surface offset coloured with the velocity explains when the flow leaves the surface and attaches back. The green part represents the flow attached to the surface, and the blue part represents the detached flow. The portion where the green and blue parts merge is where the flow attaches/detaches from the surface.

Total pressure iso-surface identifies the vortex formation, combination and separation (if it occurred). For modified (on the right) vortex of strake and wing combine and form a strong vortex which leaves the surface at a pitch down motion (Fig. 19c–19e) and then reattaches at a pitch-up motion (Fig. 19a–19c), which causes the aircraft to be slightly unstable compared to original (left sides of Fig. 19). As the vortex of wing and strake separates at a pitch up and then recombines at a pitch down but essentially remains attached to the surface (right sides of Fig. 19), original becomes more stable than modified. Finally, as the vortex breakdown of both configurations is happening away from the wing surface, they are dynamically stable at this particular Mach number and reduced frequency.

https://doi.org/10.1017/aer.2024.32 Published online by Cambridge University Press

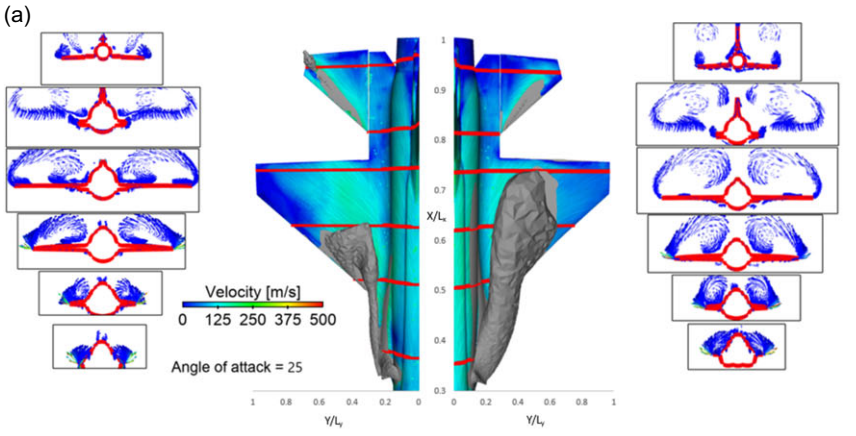

Angle of Attack=25

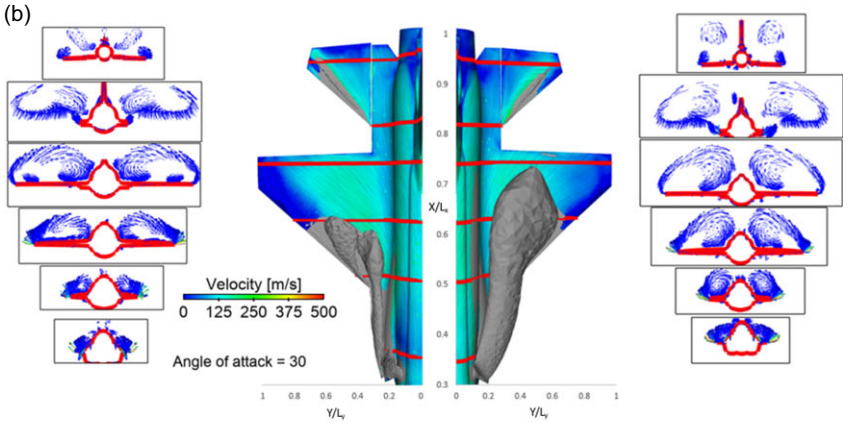

Angle of Attack=30

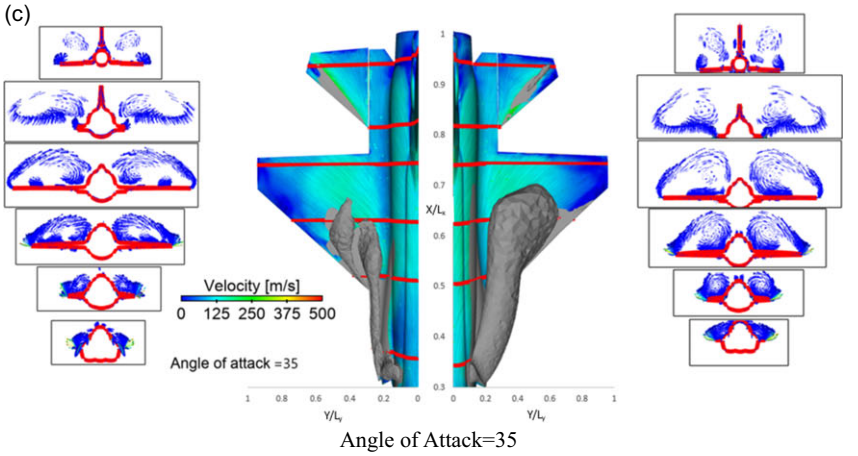

Angle of Attack=35

Figure 19. *Dynamic flow visualisation at* $Ma = 0.6$ *and* $\alpha = 30°$.

https://doi.org/10.1017/aer.2024.32 Published online by Cambridge University Press

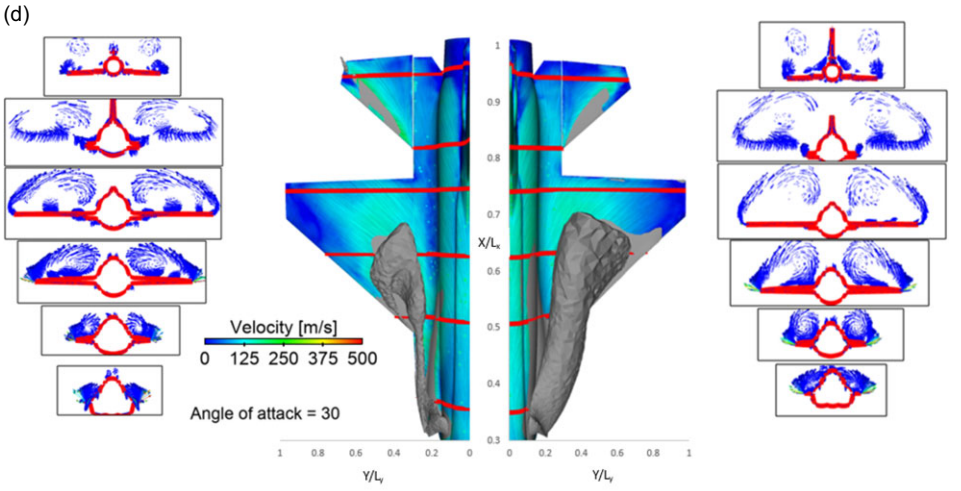

Figure 19. *Continued.*

4.0 Conclusions

Comparing the static and dynamic stability of aircraft layouts at subsonic and supersonic speeds is one of the study's goals, which was accomplished through CFD analysis. The results of this analysis show that strakes have several consequences on aircraft, which are consistent with experiments and literature.

The maximum lift of the modified configuration –which has the bigger strake – is larger at different flow Mach numbers than the original configuration – which has a shorter strake – according to the results of the static stability analysis. The original configuration appears more stable than the modified arrangement, according to the moment coefficient. When comparing a subsonic aircraft to a supersonic aircraft, it tends to be true that the two configurations become highly stable as they approach supersonic speeds.

The dynamic longitudinal stability characteristics of the original configuration display a slightly greater stability, as expected, accompanied by some discrepancies. Regarding the transition from the subsonic to the supersonic regime, both aircraft configurations are more dynamically stable in the subsonic

https://doi.org/10.1017/aer.2024.32 Published online by Cambridge University Press

regime than in the supersonic regime. Lastly, a parametric study has also shown that the original configuration is more stable than the modified configuration when the Mach number and reduced frequency change.

These observations conclude that the modified configuration demonstrates better manoeuvering capabilities than the original configuration. For a fighter aircraft, manoeuverability is a significant design consideration. The design changes have been effectively implemented on an in-service aircraft.

Acknowledgements. This work was done at the Computational Aeronautics Lab, School of Interdisciplinary Engineering and Science (SINES), NUST, Islamabad. The authors thank the support staff for providing computational resources for this research.

References

[1] Bryan G.H. Stability in aviation: an introduction to dynamical stability as applied to the motions of aeroplanes, 1911, Macmillan and Company, limited. doi: 10.1038/088406a0

[2] Nguyen L.T. Evaluation of importance of lateral acceleration derivatives in extraction of lateral-directional derivatives at high angles of attack. NASA Technical Note, NASA-TN-D-7739, 1974.

[3] Jones R.T. and Fehlner L.F. Transient effects of the wing wake on the horizontal tail. No. NACA-TN-771, 1940. https://ntrs.nasa.gov/citations/19930081625

[4] Altun M. and İyigün İ. Dynamic Stability derivatives of a manuevering combat aircraft model. *J. Aeronaut. Space Technol.*, 2004, **1**, (3), pp 19–27.

[5] Orlik-Rückemann K.J. Dynamic stability testing of aircraft—needs versus capabilities. *Prog. Aerosp. Sci.*, 1975, **16**, (4), pp 431–447. Elsevier. doi: 10.1016/0376-0421(75)90005-6

[6] Uselton B.L. and Uselton J.C. *Test Mechanism for Measuring Pitch-Damping Derivatives of Missile Configurations at High Angles of Attack*: Arnold Engineering Development Center Arnold AFB TN, 1975.

[7] Murman S. and Aftosmis M. Dynamic analysis of atmospheric-entry probes and capsules. *45th AIAA Aerospace Sciences Meeting and Exhibit*, 2007, p 74. doi: 10.2514/6.2007-74

[8] Morton S., Görtz S., McDaniel D. and Dean J. Computational aircraft and armament stability and control techniques applied to the F-16. *Proceedings of the ITEA Store Compatibility Symposium*, Destin, Florida, 2006. https://www.cobaltcfd.com/publications/

[9] Lin G. *Effects of Nonlinear Unsteady Aerodynamics on Performance, Stability and Control of an F-18 Configuration*: University of Kansas, 1997. https://www.proquest.com/openview/a6760889780fb981d41936fb4a4ec488/1?pq-origsite=gscholar&cbl=18750&diss=y

[10] Fujii K. and Schiff L.B. Numerical simulation of vortical flows over a strake-delta wing. *AIAA J.*, 1989, **27**, (9), pp 1153–1162.

[11] Lamar J.E. Analysis and design of strake-wing configurations. *J. Aircraft*, 1980, **17**, (1), pp 20–27. doi: 10.2514/3.57870

[12] Luckring J.M. Aerodynamics of strake-wing interactions. *J. Aircraft*, 1979, **16**, (11), pp 756–762. doi: 10.2514/3.58600

[13] Gursul I. and Wang Z. High angle of attack aerodynamics. *Encycl. Aerosp. Eng.*, Wiley Online Library, 2010. https://onlinelibrary.wiley.com/doi/book/10.1002/9780470686652

[14] Sedin Y.C.J., Persson I., Sillen M. and Aerosystems S. Computational analysis and re-design of a wing-strake combination, 24th International congress of the aeronautical science, ICAS 2004. https://www.icas.org/ICAS_ARCHIVE/ICAS2004/ABSTRACTS/008.HTM

[15] Ronch A.D., Vallespin D., Ghoreyshi M. and Badcock K.J. Evaluation of dynamic derivatives using computational fluid dynamics. *AIAA J.*, 2012, **50**, (2), pp 470–484.

[16] Carter D., Brandt S., Gsellman D. and Steffes J. Effects of wing sweep on stability of a 5th-generation fighter configuration, 2011. doi: 10.2514/6.2011-7037

[17] Peyrat-Armandy A. *Les avions de transport modernes & futurs*: Teknea, 1997. Amazon.com : 9782877170437.

[18] Maqsood A., Masud J. and Mehdi A. Aerodynamic evaluation of wing-strake modification by higher order panel method. *45th AIAA Aerospace Sciences Meeting and Exhibit*, Reno, Nevada, 2007, p 677. https://arc.aiaa.org/doi/abs/10.2514/6.2007-677

[19] Masud J., Malik B. and Akhtar S. Analysis of spin characteristics of a high performance aircraft with high alpha Yawing moment asymmetry. *AIAA Atmospheric Flight Mechanics Conference*, San Diego, CA, USA, 2016, p 1038. https://arc.aiaa.org/doi/abs/10.2514/6.2016-1038

[20] Wang N., Ma R., Chang X. and Zhang, L. Numerical virtual flight simulation of Quasi-Cobra maneuver of a fighter aircraft. *J. Aircraft*, 2021, **58**, (1), pp 138–152. doi: 10.2514/1.C035687

[21] Polhamus E.C. Predictions of vortex-lift characteristics by a leading-edge suction analogy. *J. Aircraft*, 1971, **8**, (4), pp 193–199.

[22] Schmidt S. and Newman D.M. Estimation of dynamic stability derivatives of a generic aircraft. *Proceedings of the 17th Australasian Fluid Mechanics Conference 2010*, Auckland, New Zealand, 2010, pp 264–267.

[23] Zhao D. and Wang J. Stability analysis and design for polynomial nonlinear systems using SOS with application to aircraft flight control. *IFAC Proc. Vol.*, 2008, **41**, (2), pp 8684–8689. Elsevier.

https://doi.org/10.1017/aer.2024.32 Published online by Cambridge University Press

APPENDIX

5.0 Detailed pitch damping derivatives calculation

The dynamic stability equations used in this work are described here. In harmonic pitching motion, pitch rate q and angle-of-attack α is given by [22].

$$\begin{aligned} \alpha(t) &= \alpha_o + \alpha_A cos(\omega t) \\ \dot{\alpha}(t) &= -\alpha_A \omega sin(\omega t) \\ q(t) &= -\alpha_A \omega sin(\omega t) \end{aligned} \tag{4}$$

Accounting for the angle-of-attack and pitch rate, the time-dependent pitching moment is:

$$\begin{aligned} C_M(t) &= C_{M_\alpha}\alpha + C_{M_{\dot{\alpha}}}\frac{\dot{\alpha}k}{\omega} + C_{M_q}\frac{qk}{\omega} \\ &= C_{M_\alpha}\alpha_A cos(\omega t) + C_{M_{\dot{\alpha}}}\frac{-\alpha_A k\omega sin(\omega t)}{\omega} + C_{M_q}\frac{-\alpha_A k\omega sin(\omega t)}{\omega} \\ &= C_{M_\alpha}\alpha_A cos(\omega t) - \left(C_{M_{\dot{\alpha}}} + C_{M_q}\right)\alpha_A k sin(\omega t) \end{aligned} \tag{5}$$

The derivatives of interest are:

$$\begin{aligned} C_{M_\alpha} &= \frac{\partial C_M}{\partial \alpha} \\ C_{M_q} &= \frac{\partial C_M}{\partial\left(\frac{qd}{2V_\infty}\right)} \\ C_{M_{\dot{\alpha}}} &= \frac{\partial C_M}{\partial\left(\frac{\dot{\alpha}}{2V_\infty}\right)} \end{aligned} \tag{6}$$

The values $k_q = \frac{qd}{2V_\infty}$ is known as reduced pitch rate. Finally,

$$C_{M_{\dot{\alpha}}} + C_{M_q} = \frac{\Delta C_M}{2k_q} \tag{7}$$

In Equation 5, higher-order terms are ignored because of the small perturbation theory. Small perturbation theory explains why we use the sum of derivatives in Equation 7. To understand that, q and $\dot{\alpha}$ are defined as:

5.1 Pitch rate (q)

The pitch rate of an aircraft is a rate of change of aircraft orientation concerning an inertial frame, expressed in the body axis; it is attributed to the additional lift on the horizontal tail due to rotation about the centre of mass.

$$C_{M_q} = -2a_t V_H \frac{l_t}{\bar{c}} \tag{8}$$

5.2 Rate of change of angle-of-attack ($\dot{\alpha}$)

The rate of change of aircraft orientation concerning the air-relative velocity, "lag of down-wash". It is an unsteady aerodynamic effect that is present in normal flight conditions.

$$C_{M_{\dot{\alpha}}} = -2a_t V_H \frac{l_t}{\bar{c}}\frac{\partial \epsilon}{\partial \alpha} \tag{9}$$

https://doi.org/10.1017/aer.2024.32 Published online by Cambridge University Press

The relation between q and $\dot{\alpha}$ is [23]:

$$\dot{\alpha} = q - \frac{\bar{q}S}{mVcos\beta}C_L + g\frac{cos\alpha cos\phi cos\theta + sin\alpha sin\theta}{Vcos\beta} - tan\beta(pcos\alpha + rsin\alpha) - \frac{X_T\, sin\alpha}{mVcos\beta} \tag{10}$$

For small perturbations, $\dot{\alpha}$ and q are practically equal because other terms have little effect on $\dot{\alpha}$, so other terms than q are negligible.

Equations 8 and 9 depict the difference between $\dot{\alpha}$ and q. Which is why dynamic combined derivative $C_{M_{\dot{\alpha}}} + C_{M_q}$ cannot be separated easily. They can be separated either by evaluating $C_{M_{\dot{\alpha}}}$ with plunging motion, or by evaluating C_{M_q} with flapping motion.

$C_{M_{\dot{\alpha}}} + C_{M_q}$ is analogous to the damping coefficient in the spring-mass-damper system. The value of this derivative means how much an aircraft can return to its original position. Unlike the damping coefficient of spring-mass-damper, the negative value of $C_{M_{\dot{\alpha}}} + C_{M_q}$ means stability, and a positive value means instability the same way as the value of C_M in static stability behaves. A more negative value means the aircraft has more ability to come back to equilibrium. Similarly, more positive means aircraft will drift away with perturbation.

Other then $C_{M_{\dot{\alpha}}} + C_{M_q}$ another derivative which is important in stability analysis is $C_{L_{\dot{\alpha}}} + C_{L_q}$. This derivative explains how much an aircraft can achieve the required lift under certain conditions. A negative value means it will quickly achieve the lift, while a positive value will diverge from the required lift. A more negative value means achieving lift faster. A more positive value means high divergence.

Cite this article: Raza H., Maqsood A. and Masud J. (2024). Altering flight stability characteristics of a high-performance aircraft through wing strake modification. *The Aeronautical Journal*, **128**, 2105–2125. https://doi.org/10.1017/aer.2024.32